Geophysical Research Letters

RESEARCH LETTER
10.1029/2020GL092150

Supraglacial Ice Cliffs Can Substantially Increase the Mass Loss of Debris-Covered Glaciers

Pascal Buri[1,2], Evan S. Miles[2], Jakob F. Steiner[3,4], Silvan Ragettli[5,6], and Francesca Pellicciotti[2,7]

[1]Geophysical Institute, University of Alaska Fairbanks, Fairbanks, AK, USA, [2]Swiss Federal Institute for Forest, Snow and Landscape Research WSL, Birmensdorf, Switzerland, [3]Faculty of Geosciences, Utrecht University, Utrecht, The Netherlands, [4]International Centre for Integrated Mountain Development, Kathmandu, Nepal, [5]Institute of Environmental Engineering, ETH Zürich, Zürich, Switzerland, [6]Hydrosolutions Ltd, Zürich, Switzerland, [7]Department of Geography, Northumbria University, Newcastle upon Tyne, UK

Key Points:

- We use a numerical model to produce the first catchment-scale study of ice cliff backwasting and contribution to glacier mass loss
- In the study catchment ice cliffs cover 2.1% ± 0.6% of debris-covered tongues but cause 17% ± 4% of their annual ice loss
- We found that cliffs enhance melt where other processes would suppress it, that is, at high elevations or where debris is thick

Supporting Information:

- Supporting Information S1

Correspondence to:
P. Buri,
pascal.buri@wsl.ch

Citation:
Buri, P., Miles, E. S., Steiner, J. F., Ragettli, S., & Pellicciotti, F. (2021). Supraglacial ice cliffs can substantially increase the mass loss of debris-covered glaciers. *Geophysical Research Letters*, *48*, e2020GL092150. https://doi.org/10.1029/2020GL092150

Received 18 DEC 2020
Accepted 10 FEB 2021

Abstract The thinning patterns of debris-covered glaciers in High Mountain Asia are not well understood. Here we calculate the effect of supraglacial ice cliffs on the mass balance of all glaciers in a Himalayan catchment, using a process-based ice cliff melt model. We show that ice cliffs are responsible for higher than expected thinning rates of debris-covered glacier tongues, leading to an underestimation of their ice mass loss of 17% ± 4% in the catchment if not considered. We also show that cliffs do enhance melt where other processes would suppress it, that is, at high elevations, or where debris is thick, and that they contribute relatively more to glacier mass loss if oriented north. Our approach provides a key contribution to our understanding of the mass losses of debris-covered glaciers, and a new quantification of their catchment wide melt and mass balance.

Plain Language Summary A significant part of glacier ice in High Mountain Asia is covered with debris, which substantially complicates the response of these glaciers to a warming climate. Projections of future glacier change are uncertain because melt and evolution of debris-covered glaciers are poorly understood. Recent research indicates that ice cliffs on debris-covered glaciers act as hot spots for melt and may contribute to anomalously high glacier mass losses. This study calculates how ice cliffs impact the mass balance of debris-covered glaciers in an entire catchment in the Nepalese Himalayas (Langtang Valley), using a model resolving cliffs melt and evolution mechanisms, high resolution topographic data, direct meteorological measurements, and satellite-based estimates of the total glacier mass balance. We show that the mass loss of debris-covered glacier tongues in the catchment would be underestimated by 17% ± 4% if ice cliffs are neglected. We conclude that ice cliffs do enhance melt where other processes would suppress it, that is, high up on the glacier, or where the debris layer is thick. By providing for the first time estimates of the catchment-wide effect of cliffs on debris-covered glaciers, this study represents a step forward in understanding their mass balance, and thus, their dynamics and surface evolution.

1. Introduction

Rock debris covers about 11% of the glacier area in High Mountain Asia (HMA), and importantly, about one third of their ice mass below the equilibrium line (Kraaijenbrink et al., 2017), that is, the area which actively contributes to melt. The timing and the quantity of melt water runoff from glaciers is increasingly important for the large and growing economies of the downstream regions of HMA (Pritchard, 2019). If supraglacial debris thickness exceeds a few centimeters, it insulates the underlying ice from the atmosphere, considerably lowering the glacier melt rate (Evatt et al., 2015; Lejeune et al., 2013; Østrem, 1959; Reid et al., 2012). Therefore debris-covered glaciers are generally thinning rather than shrinking in area and retreating (Kirkbride, 1993; Mölg et al., 2019; Ogilvie, 1904; Rowan et al., 2015; Scherler et al., 2011) but the driving mechanisms controlling the magnitude of their surface lowering are still not quantified. In recent research, steep ice faces interrupting the continuous debris layer, known as ice cliffs (Figure 1b), have been shown to substantially increase glacier melt locally (Anderson & Anderson, 2018; Bhushan et al., 2018; Han et al., 2010; Pellicciotti et al., 2015; Ragettli et al., 2016; Reid & Brock, 2014; Rounce et al., 2018; Sakai et al., 1998; Thompson et al., 2016; Watson, Quincey, Carrivick, et al., 2017). Until recently,

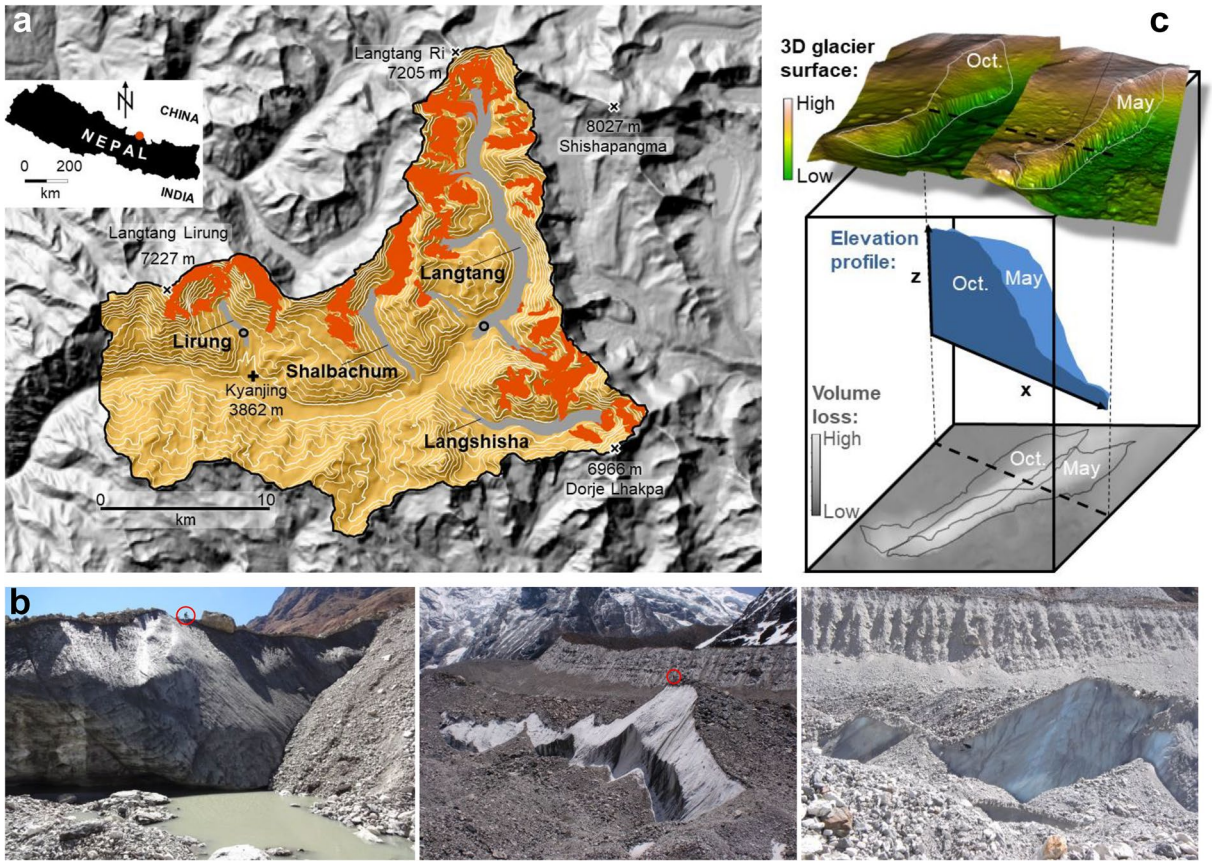

Figure 1. Map of the upper Langtang Valley catchment (a), photos showing examples of ice cliffs in the catchment (b), and visualization of ice cliff backwasting (c). (a) The catchment is indicated in yellow, glacierized areas in orange and debris in gray. The four main glaciers are Lirung, Shalbachum, Langtang, and Langshisha Glacier. Also indicated are the automatic weather stations on Lirung and Langtang Glacier (black circles) and in Kyanjing (black cross). (b) Photos of cliffs on Lirung (left) and Langtang Glacier (middle and right) with a person in red circles for scale. (c) Visualization of ice cliff backwasting based on high-resolution UAV-DEM-observations. The upper plot shows the observed 3D-evolution of a cliff on Lirung Glacier from May to October 2013 (right to left); the central plot shows in blue the observed cliff profiles at the dashed transect line in May (light) and October (dark), and in gray, the observed volume loss derived from DEM-differencing (all dimensionless). DEM, digital elevation model; UAV, unpiloted aerial vehicle.

these features could not be monitored in satellite images because of their coarse resolution and direct field observations are rare (Sakai et al., 1998). As a result, no models of glacier changes and high mountain hydrology included their effect explicitly to date. In the past few years, photogrammetric measurements (Brun et al., 2016; Watson, Quincey, Smith, et al., 2017) and detailed local energy balance modeling efforts (Buri, Miles, et al., 2016) have quantified volume losses and backwasting evolution of *individual* ice cliffs, identifying that these bare ice features can act as local hot spots for melt on debris-covered glacier tongues, melting at rates 3–14 times the rest of the ablation area (Brun et al., 2016; Buri, Pellicciotti, et al., 2016; Reid & Brock, 2014; Sakai et al., 2000; Thompson et al., 2016). These small-scale studies however are difficult to extrapolate and we therefore still lack understanding of their role on the glacier mass balance and whether they substantially alter glacier mass losses or remain confined to specific local phenomena. Here we provide the first assessment of their role at the glacier and catchment scale relevant for understanding the mass balance and hydrology of Himalayan glaciers.

Ice cliff melt for *individual* glaciers has been estimated extrapolating point-scale model results (Han et al., 2010; Reid & Brock, 2014; Sakai et al., 1998) or by differencing of digital elevation models (DEMs) (Brun et al., 2018; Thompson et al., 2016). Modeling efforts to date assumed simplified and invariant cliff geometries, neglecting complex melt patterns on the cliff surface (Buri, Miles, et al., 2016; Buri, Pellicciotti, et al., 2016) while DEM-differencing is restricted to the availability of remote sensing data and their temporal and spatial resolution and cannot provide insights into the physics of cliff mass loss. Methods relying on observational data alone additionally have to deal with glacier dynamics which are difficult to separate from

cliff backwasting (Brun et al., 2018). Modeling offers the way forward to understand the physical mechanisms controlling melt patterns over a season or beyond for future projections.

Here, we simulate the backwasting of all the cliffs in a 585 km^2 catchment containing four major debris-covered glaciers (Figure 1a) over one ablation season and we assess their contribution to the total glacier mass loss in the catchment, estimated with the mean surface mass balance rate over the period 2006–2015 and mean debris-covered area emergence velocity for the same glaciers. This allows us to reveal the importance of supraglacial ice cliffs for glacier mass loss in a Himalayan catchment. We are able to resolve the preferential orientation of ice cliffs and their effects as we analyze the cliffs' area, aspect and volume loss of an entire catchment in a consistent way. This is the first time that an ice cliff model is applied to the entire population of cliffs in a large catchment containing multiple glaciers.

2. Methods

2.1. Dynamic 3D-Backwasting Model

We assess the melt and mass loss of 366 supraglacial ice cliffs in the Langtang catchment (13% glacierized, of which one third is debris-covered), distributed on its four principal debris-covered glaciers, Lirung, Shalbachum, Langshisha, and Langtang Glacier (Figure 1a). We run an energy-balance driven, process-based 3D-backwasting model (Buri, Miles, et al., 2016) that is able to reproduce the cliff's heterogeneous melt patterns, volume loss and dynamic evolution (expansion, shrinkage and reburial), and use a Monte Carlo approach to estimate the uncertainty in key model parameters. The model, coded in the programming language R (R Core Team, 2019) has previously been used to simulate the evolution of few selected ice cliffs on Lirung Glacier (one of the study glaciers) and has been validated with multiple independent datasets (ablation stakes, terrestrial, and airborne photogrammetric surveys; Buri, Miles, et al., 2016). Average deviations between modeled and observed cliff characteristics after one melt season were all within a plausible range (10% in volume loss; 6° in mean aspect, 6% in mean slope, 9% in vertical extent, 7% in horizontal extent; Tables 3 and 4 in Buri, Miles, et al., 2016), lending confidence to its use for this application. Details of the model can be found in Buri, Miles, et al. (2016), where the model was presented and tested in detail for four cliffs on Lirung Glacier, as well as in Buri and Pellicciotti (2018), where the model was applied to two cliffs on Lirung glacier to study the effect of orientation on the survival of cliffs. In the supporting information (SI) document we only recall the changes we have implemented for this study (Section S2.4).

Initial ice cliff topographies are defined using a DEM of 3 m spatial resolution derived from SPOT6 tri-stereo satellite imagery (Ragettli et al., 2016) from April 21, 2014 and manually delineated cliff outlines based on an orthoimage of 1.5 m spatial resolution processed from the same data set (Steiner et al., 2019; Section S2.1). Simulated cliff melt is based on surface energy balance calculations (Section S2.3), in which the complex radiation patterns due to the heterogeneous ice cliff and glacier surface topographies are modeled in high detail. The surface energy balance at the cliff-atmosphere interface is calculated from energy balance equations for every grid cell, based on hourly meteorological data distributed from automatic weather stations (Section S2.2) in the catchment (Figure 1a), of which two were recording directly on the glacier surface and one off-glacier, starting on May 11, 2014 and ending on 9 October of the same year. Computation of radiative fluxes accounts for direct and diffuse components from the sky and the surrounding debris. Reflected shortwave radiation is controlled by constant ice and debris albedo values. Longwave radiation emitted from debris, sky and the ice cliff is included in the energy balance calculations. Cliffs' geometries, initiated with given cliff outlines and glacier surface topography from observational data, are adjusted twice (1 August and 9 October; this time interval was the most appropriate from consideration of model resolution and magnitude of the melt vectors) during the ablation season based on the differential ablation of the ice cliff surface, in combination with the slope and aspect of each cliff cell. The 3D-updates of the cliffs take into account (a) thermo-erosional melt at cliff-water contact zones by adjacent supraglacial ponds, a process that maintains steep sections at the cliff bottom (Brun et al., 2016; Miles et al., 2016); and (b) expansion and shrinkage of cliffs (e.g., reburial by debris), depending on the slope and the amount of debris seen at the cliff margin (Buri, Miles, et al., 2016). Steep areas above the 35° slope threshold at the ice-debris transition zone become debris-free, and shallow zones below the slope threshold along the cliff margin can become debris-covered, which allows a dynamic extension or shrinking of the ice cliff shape after the two geometry update steps during the modeling period. Subdebris melt of the surrounding glacier surface (a constant

value in time and space) is taken into account and subtracted from every off-cliff grid cell on the glacier. We excluded terminal ice cliffs from all our analysis, as they undergo different dynamics (Steiner et al., 2019).

2.2. Glacier Mass Balance Estimates

Total glacier mass loss was determined from the geodetic thinning estimates calculated for 2006–2015 spatially distributed on a 30 m resolution grid (Ragettli et al., 2016). We used the ensemble mean of the elevation differences between six DEMs (2006, 2009, 2014, and February and October 2015; Section S3.1). We corrected the observed geodetic thinning rates for emergence velocity calculated from flux gates at an interval of 50 m elevation (following the approach in Miles et al., 2018, Figure S4) to convert thinning into average annual surface mass balance rates. This approach provides estimates of surface mass balance for the four study glaciers averaged over a period of 10 years (2006–2015). Since we compare simulated ice cliffs from one season (2014) against the mean geodetic mass balance over 10 years, we first carry out an analysis of the meteorological conditions of that year in comparison to the entire period (Section S3.2). We use monthly ERA5-Land reanalysis data (Copernicus Climate Change Service, 2019) to calculate standardized anomalies of air temperature and precipitation during the 10-year period for the Langtang Area (Figure S5, Table S5). The deviation in air temperature and precipitation of our target year 2014 was small compared to the ensemble period. We thus expect the ensemble mean glacier mass balance estimate over the period to represent the 2014 mass balance well, and use it to calculate the cliffs contribution to the total glacier mass losses. Additionally we also assessed how 2014 deviates in comparison with the 10-year mean in terms of radiative forcing (Figure S5), since cliff melt is especially sensitive to short- and longwave radiation inputs. The ERA5-Land radiation estimates for 2014 do not differ significantly from the other years (Table S5) and we therefore expect that the cliff melt estimates for that particular year are representative for the 10-year period.

2.3. Uncertainty

There are multiple uncertainties in our approach: uncertainties associated to the ice cliff- and glacier areas, the selection of specific parameters in the ice cliff model and the meteorological input variables, as well as those associated to the estimates of the geodetic thinning and the emergence flux rates. We estimated these uncertainties and propagated them throughout our analysis based on the assumption of uncorrelated and random errors (Section S4). To investigate the influence of ice cliff model parameters on cliff volume loss, we randomly selected a subset of 40 cliffs which represents the whole population well in terms of distributions of slope, aspect, elevation, and area and spatial distribution (Section S4.1; Figure S6). This enabled repeated testing of the model, which is not computationally possible for the entire set. To identify the parameters whose uncertainty will have the strongest effect on the final model uncertainty, we applied a one-at-a-time sensitivity analysis by running the ice cliff model for the 2014 melt season on the cliff subset varying each parameter two times to the limits of their likely range (Figures S7 and S8). In this way, we selected the four physical model parameters debris albedo, debris emissivity, terrain slope threshold, aerodynamic roughness length, and the six meteorological input variables incoming longwave and shortwave radiation, relative humidity, air and surface temperature, and wind speed, which all have non-negligible effects over their ranges. We then carried out a Monte Carlo analysis, running 100 distinct model simulations of 40 cliffs (~10% of our total population), and assuming they have an uniform distribution, to produce an uncertainty estimate of cliff melt (Table S1). For the error estimates in glacier mass balance, we used the uncertainties of the 2006–2015 ensemble mean elevation differences (see Table 4 in Ragettli et al., 2016). Additionally we added the corresponding emergence flux uncertainties (see Table 1 in Miles et al., 2018) for each glacier. By applying 10 m buffers (inside and outside) to the actual 2014 glacier and debris outlines, we derived the areal uncertainty of glacier and debris areas (mean deviation) in the catchment. Cliff area delineation uncertainty was previously estimated to be 26% in Steiner et al. (2019) as a result from manual delineation and stereo image quality.

3. Results

3.1. Ice Cliff Backwasting and Characteristics

The simulations revealed average ice cliff backwasting in the order of 5–10 m in horizontal direction during the melt season. The modeled mean daily sums of energy fluxes (Figure S1) reveal insights into the mechanisms of ice cliff backwasting: none of the fluxes shows a clear trend with elevation, defying simple elevation-based parameterizations. Latent heat LE is the only energy flux which changes from slightly positive to slightly negative with elevation, as a function of the temperature lapse rate. Thus, air temperature does not seem to be the main control of cliffs backwasting. This implies that the energy balance resulting from the interactions of fluxes is complex and not easily prone to parameterizations, and likely dominated by radiative fluxes (Figure S1). The number of cliffs varies greatly between glaciers and decreases slightly over the season according to the simulations (from 366 to 322) and the cliffs become slightly steeper from May to October (Figure S2). With the exception of one 50 m-elevation segment on Langshisha Glacier, where the tongue is relatively narrow and ice cliffs occupied 8.6% of the glacier area, the relative areal contribution per elevation segment never exceeds 4.3% (Langtang), 2.6% (Lirung), or 2.8% (Shalbachum) on the four glaciers (Figure 2, and Tables S6–S9).

3.2. Cliffs Contribution to Glacier Mass Losses

We present the cliff backwasting results as a relative contribution to mean glacier mass balance spatially across each glacier (Figure 2, M). Cliffs are substantial contributors to the melt of debris-covered glacier tongues. The total mass losses attributable to cliffs are $5.2 \times 10^{-3} \pm 1.2 \times 10^{-3}$ km^3 w.e. over the melting season from May 11 to October 9, 2014 (Table 1). This is equivalent to 0.22 ± 0.05 m w.e. thinning in the Langtang catchment over the same period (0.07 ± 0.02 m w.e. thinning of the entire glaciers; Table S10). We convert these values into portions of total geodetic glacier mass loss rates. Although the debris-covered glacier tongues have only 2.1% ± 0.69% of their surface area exposed to the atmosphere as ice cliffs, they account for 17% ± 4% of the mass loss of the debris-covered tongues in the catchment (Table 1). Considering the glacier area of the entire catchment, the 0.6% ± 0.2% area of ice cliff accounts for 15% ± 5% of glacier mass loss.

The very high melt efficiency of cliffs compared to their small area can be expressed through an enhancement factor (Figure 2, EF, and Table 1), which we define as the ratio of the relative contributions of ice cliff volume loss and ice cliff area (Brun et al., 2018) (Equation 6 in SI). The EFs obtained in this way vary between 6 ± 3 on Langshisha Glacier and 13 ± 4 on Langtang Glacier and indicate very high efficiency of ice cliff backwasting compared to the debris-covered area's mass loss. Despite a relative ice cliff coverage of less than 1% at the glacier scale, these bare-ice surface features are responsible for 7% ± 4% (Shalbachum Glacier) to 17% ± 5% (Langtang Glacier) of the net mass loss of the entire glacier for the model period, indicating that ice cliff melt is 18 ± 12 (Shalbachum Glacier) to 67 ± 64 times (Lirung Glacier) higher than the melt of the rest of the glacier (subdebris melt, bare ice melt and accumulation higher up combined).

Cliff-associated volume losses vary considerably from glacier to glacier and are dominated by Langtang and Langshisha Glacier because of their larger size. Corresponding cliff-associated melt on these two tongues is −0.24 ± 0.05 and −0.21 ± 0.06 m w.e. relative to planimetric surface area, respectively (Table S10). The ice cliffs contribute most in terms of mass loss in the lower and upper sections of the glaciers and show a reduction in the middle zones of the glacier tongues. Although the debris-covered tongues have similar fractions of ice cliff area exposed to the atmosphere (between 1.6% ± 0.4% on Lirung Glacier and 2.7% ± 0.7% on Langshisha Glacier, Table 1), the relative importance of ice cliff melt for net glacier mass loss greatly differs (Table 1) because of differences in debris thickness, subdebris melt and elevation. On all four glaciers single elevation bands show relative volume losses attributable to ice cliffs > 10%, and Langshisha and Langtang glaciers reach contributions of > 40% in their lowermost sections, where the debris layer is thickest, or on glacier tributaries which are prone to avalanches. Both thick debris and avalanches result in a less negative mass balance, because of reduced melt or increased accumulation.

Superimposed on this spatial pattern, cliffs' aspect appears to exert a strong control on mass losses, with the highest volume losses at northwest-oriented cliffs on all four glaciers (Figure 3), despite the glaciers'

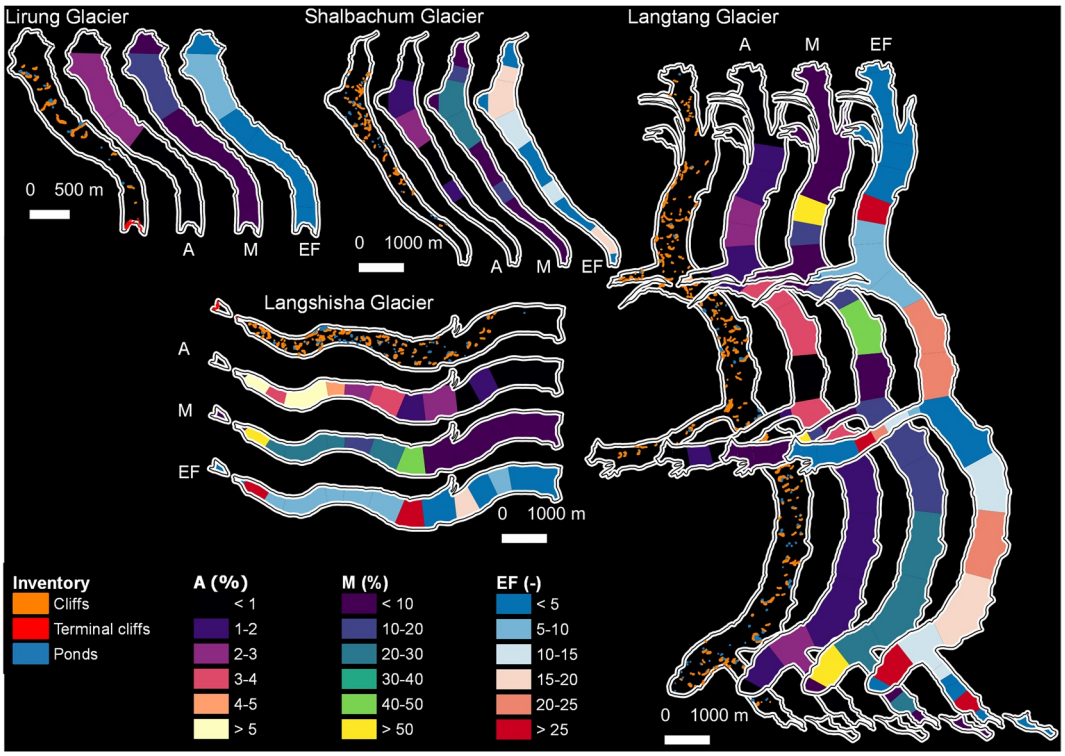

Figure 2. Cliff and pond observations and model results per elevation band in the Langtang Valley catchment. Lirung Glacier, Shalbachum Glacier, Langshisha Glacier, and Langtang Glacier with debris covered tongues (white outline), supraglacial ice cliffs (orange), and ponds (blue). Terminal ice cliffs are indicated in red. The relative contribution of ice cliffs in terms of observed area (A) and modeled mass balance (M) compared to the glacier per 50 m-elevation segment are shown in the next two glacier shapes. The shape to the right shows the enhancement factor (EF), indicating the ratio of A to M (efficiency of ice cliff melt compared to glacier mass loss per unit area).

contrasting overall flow directions. This supports previous findings that ice cliffs in the Langtang catchment find their ideal aspect in terms of survival time and area in a northwest orientation (Buri & Pellicciotti, 2018; Steiner et al., 2019). South- and east-facing ice cliffs are thus negligible at the glacier- and catchment scale on the glaciers of Langtang Valley. Cliffs facing these aspects may be more prevalent and more important in other catchments if independent controls (e.g., supraglacial streams or crevasses) are able to maintain their geometry and aspect.

4. Discussion and Conclusions

We found that cliffs enhance melt especially where this would normally be reduced by the environmental conditions, that is: (1) at high elevations and (2) where debris is thick (i.e., several decimeters; Figure 4), thus providing a mechanism that drives ablation through absorption of solar radiation. Case (1) is evident on Langtang Glacier, which shows the highest contribution of ice cliffs to total glacier melt (21% ± 4%; Table 1), exceeding 13 ± 4 times the cliff area. This high contribution of cliffs to total mass losses is due to the glacier's higher elevation and associated lower glacier-wide sub-debris melt rates on the tongue (−1.17 ± 0.06 m w.e.; Table S10), compared to the other three glaciers in this study. Glacier melt rates on the upper debris zones of Langtang Glacier (reaching above 5,300 m a.s.l.) are reduced by low air temperatures that results in strong radiative losses at the debris surface and low energy available for melt of the debris-covered ice. On ice cliffs, instead, because of their inclined surfaces, the energy available for melt is less sensitive to elevation (Figure S1) and is instead controlled by incident radiation. The relative contribution of cliffs to glacier mass loss thus increases toward the upper reaches of the glacier tongue on all four glaciers (Figure S3). Case (2) is evident on the terminus of all four glaciers, where debris is thickest, and for Lirung on the entire glacier because of a rather thick debris layer throughout (Figure S3). The combination

Table 1
Ice Cliffs Area and Volume Losses for All the Cliffs Per Glacier and Overall

		Langtang	Lirung	Langshisha	Shalbachum	Σ
Number of cliffs	n_{cl}	225	17	79	45	366
Area abs. (km^2)	A_{gl}	46.5 ± 1.9	6.5 ± 0.5	16.3 ± 0.7	10.2 ± 0.4	79.5 ± 3.4
	A_{deb}	15.5 ± 0.7	1 ± < 0.1	4.5 ± 0.2	2.6 ± 0.1	23.7 ± 1.1
	A_{cl}	$3.1 \times 10^{-1} \pm 8.1 \times 10^{-2}$	$1.8 \times 10^{-2} \pm 4.7 \times 10^{-3}$	$1.2 \times 10^{-1} \pm 3.1 \times 10^{-2}$	$4.4 \times 10^{-2} \pm 1.1 \times 10^{-2}$	$5.0 \times 10^{-1} \pm 1.3 \times 10^{-1}$
A_{cl} rel. to A_{gl} (%)	$A_{rel,gl}$	0.7 ± 0.2	0.3 ± 0.1	0.7 ± 0.2	0.4 ± 0.1	0.6 ± 0.2
A_{cl} rel. to A_{deb} (%)	$A_{rel,deb}$	2.0 ± 0.5	1.6 ± 0.4	2.7 ± 0.7	1.7 ± 0.4	2.1 ± 0.6
Volume loss abs. (km^3 w.e.)	V_{gl}	$-2.2 \times 10^{-2} \pm 5.1 \times 10^{-3}$	$-1.2 \times 10^{-3} \pm 8.8 \times 10^{-4}$	$-6.2 \times 10^{-3} \pm 2.6 \times 10^{-3}$	$-4.6 \times 10^{-3} \pm 1.7 \times 10^{-3}$	$-3.4 \times 10^{-2} \pm 6.1 \times 10^{-3}$
	V_{deb}	$-1.8 \times 10^{-2} \pm 8.9 \times 10^{-4}$	$-1.8 \times 10^{-3} \pm 5.8 \times 10^{-4}$	$-6.6 \times 10^{-3} \pm 1.0 \times 10^{-3}$	$-3.2 \times 10^{-3} \pm 4.7 \times 10^{-4}$	$-3.0 \times 10^{-2} \pm 1.5 \times 10^{-3}$
	V_{cl}	$-3.7 \times 10^{-3} \pm 7.6 \times 10^{-4}$	$-1.9 \times 10^{-4} \pm 5.7 \times 10^{-5}$	$-9.4 \times 10^{-4} \pm 2.7 \times 10^{-4}$	$-3.4 \times 10^{-4} \pm 1.5 \times 10^{-4}$	$-5.2 \times 10^{-3} \pm 1.2 \times 10^{-3}$
V_{cl} rel. to V_{gl} (%)	$V_{rel,gl}$	17 ± 5	16 ± 12	15 ± 8	7 ± 4	15 ± 5
V_{cl} rel. to V_{deb} (%)	$V_{rel,deb}$	21 ± 4	11 ± 5	14 ± 5	10 ± 5	17 ± 4
EF per unit A_{gl} (–)	EF_{gl}	31 ± 14	67 ± 64	24 ± 15	18 ± 12	29 ± 12
EF per unit A_{deb} (–)	EF_{deb}	13 ± 4	7 ± 4	6 ± 3	7 ± 4	10 ± 4

Notes. Area values are based on the cliff inventory, while volume losses are modeled using the ice cliff backwasting model run for the period from May to October 2014. Subscripts gl and deb refer to the entire glacier surface and the debris-covered tongue only, respectively. Total glacier volume losses used to calculate the percentage contribution of cliffs to total mass balance are estimated using the sum of observed ensemble mean geodetic thinning rates 2006–2015 (Ragettli et al., 2016) and modeled emergence fluxes for the same period (Miles et al., 2018). The so-called enhancement factor (EF) indicates the ratio of the relative cliff melt contribution to the relative cliff area (Section S5). All values are rounded to two significant digits where applicable.

of the two cases, with the ice cliffs acting as melt hotspots that amplify melt where it would be otherwise suppressed (by either thick debris lower down or cold conditions higher up), create the double peak evident in the EF along the glacier tongue (Figure 2 and Figure S3).

We provide the first catchment scale model-based evidence of the substantial contribution of ice cliffs, a key component of debris-covered glacier mass losses, to total ablation. For all the debris-covered glacier tongues in the high-elevation Langtang catchment, 17% ± 4% (0.22 ± 0.05 m w.e.) of glacier mass loss during one normal ablation season is attributable to ice cliff melt. The catchment-wide glacier melt is underestimated by roughly 15% ± 5% if ice cliff melt is not considered. Our independent approach clearly isolates the melt attributable to cliffs and is consistent with detailed measurements at one of the studied glaciers (Brun et al., 2016). Glacier-scale remote sensing efforts to assess cliff influence have generally led to lower-end estimates of cliff melt enhancement factors (Brun et al., 2018; Mölg et al., 2019), but crucially depend on the successful identification of all cliff melt-affected areas between observations; the challenges in successfully identifying cliffs in a variety of illumination conditions, even from high-resolution imagery (Kneib et al., 2020; Steiner et al., 2019; Thompson et al., 2016; Watson et al., 2016) biases remote sensing assessments of cliffs' influence to lower values. Furthermore, such estimates are strongly influenced by estimation of glacier emergence velocity and its spatial pattern, or lack thereof.

Our study shows that ice cliff backwasting is a non-negligible term in the total glacier mass balance of these Himalayan debris-covered glaciers: in our study catchment 15% ± 5% of the total net ice loss of the four study glaciers (equivalent to a surface thinning of 0.07 ± 0.02 m w.e.) can be attributed to ice cliff melt, although the cliffs cover only 0.6% ± 0.2% of the glacier area (EF = 29 ± 12). This reveals the efficiency of their backwasting mechanism compared to subdebris melt. Ice cliffs have often been associated with supraglacial ponds, which also act as melt hotspots (Miles et al., 2016; Sakai et al., 2000; Watson, Quincey,

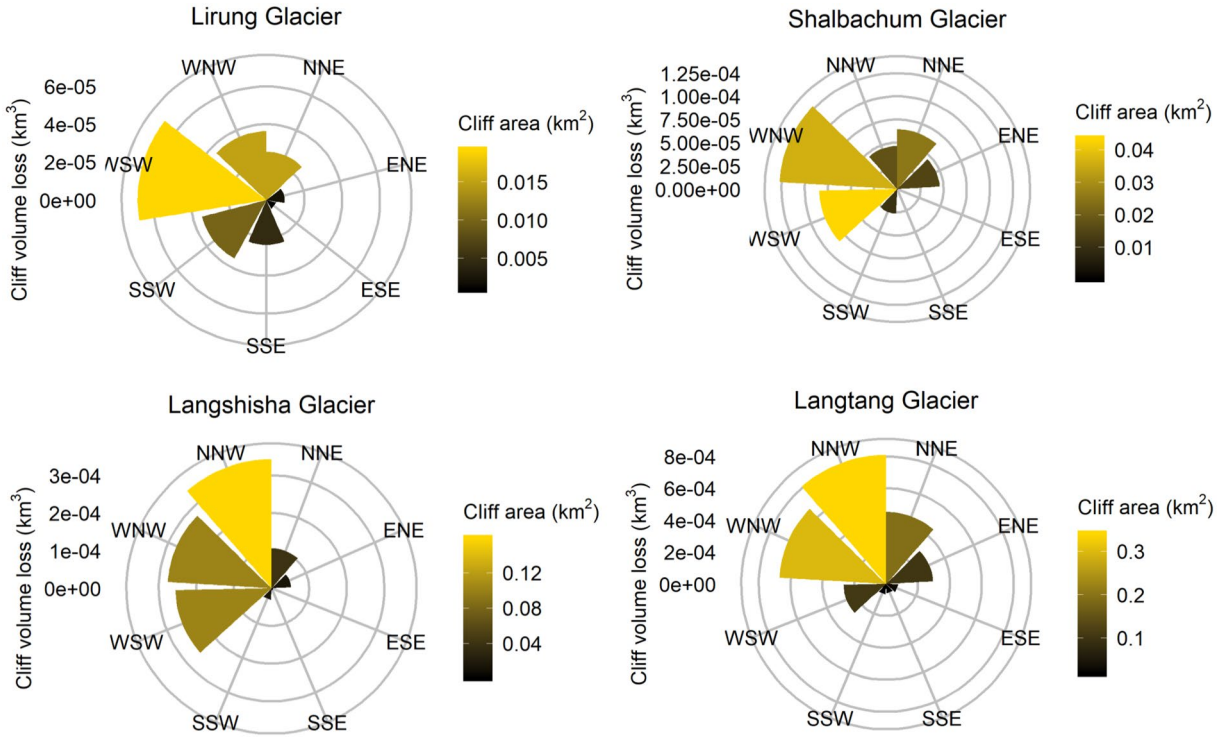

Figure 3. Model results per aspect for four debris-covered glaciers in the Langtang Valley catchment. Total volume losses of ice cliffs per aspect (45°-sections) for the four glaciers shown in Figures 1a and 2. The color, direction, and size of the pie chart pieces indicate area, aspect and volume loss of all cliffs summarized per 45°-aspect section.

Carrivick, et al., 2017). For the same catchment, Miles et al. (2018) estimated that ponds cover 1.0% of the debris-covered area, yet contribute to 13.8% ± 2.9% of the annual mass loss. If we combine this estimate with our own, we find that the 97% ± 0.7% covered by debris contributes 69% ± 5% of ice mass loss. Together, cliffs and ponds cover 3.1% ± 0.7% of the area but contribute 31% ± 5% to mass loss, showing a net effective enhancement factor of 14 ± 6. This is a conservative estimate, as it is based on an inventory of cliffs from which we have removed all features where there was some uncertainty in delineation (Steiner et al., 2019; Section S7). Further we likely miss a few weeks of ice cliff melt before and after the ice cliff model period, which would also slightly raise the relative contribution of ice cliff melt to glacier mass loss at the annual basis. We estimate the ice cliff melt during the shoulder seasons to be less than 18% compared to the ice cliff melt during the model period at the lowest elevation in the catchment and less than 2% above the average elevation of the cliff domain (Section S6).

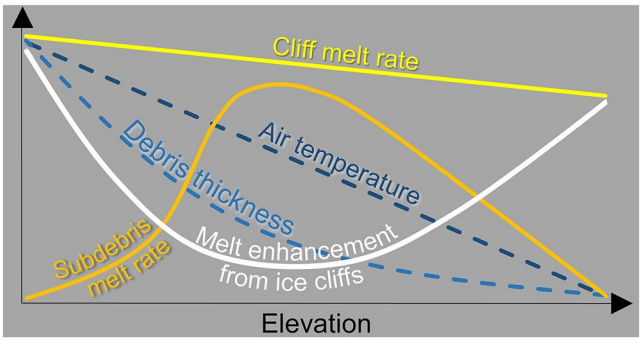

Figure 4. Conceptual scheme of the main controls of debris-covered glaciers mass losses and their variations with elevation. Variations with elevation of air temperature (environmental lapse rate, e.g., Steiner & Pellicciotti, 2016), debris thickness (e.g., Anderson & Anderson, 2016), subdebris melt rate, ice cliff melt rate, and melt enhancement from ice cliffs over debris-covered glacier tongues (this study), independent of the number of cliffs.

We do not account for cliffs emerging within the melt season and we do not include the melt influences of supraglacial streams, which can be relevant surface features on debris-covered glaciers with different morphologies and debris cover and should be studied in future research. Further the direct comparison of ice cliff melt over one melt season only with the annual glacier mass balance estimates can be slightly convoluted by the presence of snow accumulation at the glacier scale.

The relative debris-cover extent on glaciers in HMA and in glacierized areas globally is likely to increase in a warming climate (Herreid & Pellicciotti, 2020; Scherler et al., 2018). Shrinking glaciers uncover new source areas for debris supply and increase the gravitational potential between the source and the glacier surface, as well as exposing increasingly larger amounts of englacial debris. In this context, the importance

of supraglacial melt hot spots such as ice cliffs will increase. The glaciers in the Langtang catchment are all in a rather advanced evolutionary stage (stage values between 0.71 and 0.78; from Herreid & Pellicciotti, 2020) in terms of debris cover, decay and stagnancy, with extensive (and possibly thick) debris cover that have almost reached the (areal) carrying capacity of the glaciers. They are examples of how glaciers in earlier stages and similar environments might look like in the future. Our findings show that on glaciers in an advanced debris stage, cliffs will act as a dominant mechanism of glacier ablation, even despite their small number, confirming findings from Ngozumpa Glacier (Khumbu Region, Nepal; stage value = 0.78) (Thompson et al., 2016). A better understanding of the sourcing and temporal and spatial evolution of debris volumes on glaciers, in combination with the appearance, life cycle and decay of supraglacial ice cliffs, seem imperative to simulate the dynamics, mass losses, and streamflow contribution of increasingly prevalent debris-covered glaciers.

Data Availability Statement

Model results of this study are archived and available at Zenodo (*Langtang Ice Cliff Modeling Study*; http://doi.org/10.5281/zenodo.4073138), the ice cliff inventory is openly accessible via Pangaea (https://doi.pangaea.de/10.1594/PANGAEA.899171) from Steiner et al. (2019).

Acknowledgments
The authors thank Tek Rai and his logistics team, as well as Simon Wicki, Anna Chesnokova, Ian Willis, Ibai Rico, and Peter Hill for the help during our field work in Langtang Valley in May and October 2014. The authors acknowledge the efforts of Walter Immerzeel, Joseph Shea, and ICIMOD to install and maintain a meteorological network in the Langtang Valley, which we used to complement our on-glacier stations. This study was funded by the SNF-project *UNCOMUN* (grant no. 146761) and the ERC-project *RAVEN* (grant no. 772751) under the European Union's Horizon 2020 research and innovation program. Pascal Buri acknowledges funding from the SNF Early Postdoc.Mobility program (grant no. 178420). The views and interpretations in this study are those of the authors and are not necessarily attributable to ICIMOD. The authors want to thank the Scientific Editor M. Morlighem, and three anonymous reviewers for their thorough and helpful comments, which greatly improved the paper.

References

Anderson, L. S., & Anderson, R. S. (2016). Modeling debris-covered glaciers: response to steady debris deposition. *The Cryosphere*, *10*(3), 1105–1124. https://doi.org/10.5194/tc-10-1105-2016. Retrieved from http://www.the-cryosphere.net/10/1105/2016/

Anderson, L. S., & Anderson, R. S. (2018). Debris thickness patterns on debris-covered glaciers. *Geomorphology*, *311*, 1–12. https://doi.org/10.1016/j.geomorph.2018.03.014

Bhushan, S., Syed, T. H., Arendt, A. A., Kulkarni, A. V., & Sinha, D. (2018). Assessing controls on mass budget and surface velocity variations of glaciers in Western Himalaya. *Scientific Reports*, *8*(1). https://doi.org/10.1038/s41598-018-27014-y

Brun, F., Buri, P., Miles, E. S., Wagnon, P., Steiner, J. F., Berthier, E., et al. (2016). Quantifying volume loss from ice cliffs on debris-covered glaciers using high-resolution terrestrial and aerial photogrammetry. *Journal of Glaciology*, 1–12. https://doi.org/10.1017/jog.2016.54

Brun, F., Wagnon, P., Berthier, E., Shea, J. M., Immerzeel, W. W., Kraaijenbrink, P. D. A., et al. (2018). Ice cliff contribution to the tongue-wide ablation of Changri-Nup Glacier, Nepal, central Himalaya. *The Cryosphere*, *12*(11), 3439–3457. https://doi.org/10.5194/tc-12-3439-2018

Buri, P., Miles, E. S., Steiner, J. F., Immerzeel, W. W., Wagnon, P., & Pellicciotti, F. (2016). A physically based 3-D model of ice cliff evolution over debris-covered glaciers. *Journal of Geophysical Research: Earth Surface*, *121*(12), 2471–2493. https://doi.org/10.1002/2016JF004039

Buri, P., & Pellicciotti, F. (2018). Aspect controls the survival of ice cliffs on debris-covered glaciers. *Proceedings of the National Academy of Sciences of the United States of America*, *115*(17), 4369–4374. https://doi.org/10.1073/pnas.1713892115

Buri, P., Pellicciotti, F., Steiner, J. F., Miles, E. S., & Immerzeel, W. W. (2016). A grid-based model of backwasting of supraglacial ice cliffs on debris-covered glaciers. *Annals of Glaciology*, *57*(71), 199–211. https://doi.org/10.3189/2016AoG71A059

Copernicus Climate Change Service. (2019). *ERA5-land hourly data from 2001 to present*: ECMWF. https://doi.org/10.24381/CDS.E2161BAC

Evatt, G. W., Abrahams, I. D., Heil, M., Mayer, C., Kingslake, J., Mitchell, S. L., et al. (2015). Glacial melt under a porous debris layer. *Journal of Glaciology*, *61*(229), 825–836. https://doi.org/10.3189/2015JoG14J235. Retrieved from https://academiccommons.columbia.edu/catalog/ac:195906

Han, H., Wang, J., Wei, J., & Liu, S. (2010). Backwasting rate on debris-covered Koxkar glacier, Tuomuer mountain, China. *Journal of Glaciology*, *56*(196), 287–296. https://doi.org/10.3189/002214310791968430

Herreid, S., & Pellicciotti, F. (2020). The state of rock debris covering Earth's glaciers. *Nature Geoscience*. https://doi.org/10.1038/s41561-020-0615-0

Kirkbride, M. P. (1993). The temporal significance of transitions from melting to calving termini at glaciers in the central Southern Alps of New Zealand. *The Holocene*, *3*(3), 232–240. Retrieved from http://hol.sagepub.com/cgi/doi/10.1177/095968369300300305. https://doi.org/10.1177/095968369300300305

Kneib, M., Miles, E., Jola, S., Buri, P., Herreid, S., Bhattacharya, A., et al. (2020). Mapping ice cliffs on debris-covered glaciers using multispectral satellite images. *Remote Sensing of Environment*, *253*, 112201. Retrieved from http://www.sciencedirect.com/science/article/pii/S0034425720305745. https://doi.org/10.1016/j.rse.2020.112201

Kraaijenbrink, P. D. A., Bierkens, M., Lutz, A., & Immerzeel, W. (2017). Impact of a global temperature rise of 1.5 degrees Celsius on Asia glaciers. *Nature*, *549*(7671), 257. https://doi.org/10.1038/nature23878

Lejeune, Y., Bertrand, J.-M., Wagnon, P., & Morin, S. (2013). A physically based model of the year-round surface energy and mass balance of debris-covered glaciers. *Journal of Glaciology*, *59*(214), 32744. https://doi.org/10.3189/2013JoG12J149

Miles, E. S., Pellicciotti, F., Willis, I. C., Steiner, J. F., Buri, P., & Arnold, N. S. (2016). Refined energy-balance modelling of a supraglacial pond, Langtang Khola, Nepal. *Annals of Glaciology*, *57*(71), 29–40. https://doi.org/10.3189/2016aog71a421

Miles, E. S., Willis, I., Buri, P., Steiner, J. F., Arnold, N. S., & Pellicciotti, F. (2018). Enhanced energy absorption by supraglacial ponds accounts for 1/8 of total ice loss from five himalayan debris covered glaciers. *Geophysical Research Letters*. https://doi.org/10.1029/2018GL079678

Mölg, N., Bolch, T., Walter, A., & Vieli, A. (2019). Unravelling the evolution of Zmuttgletscher and its debris cover since the end of the Little Ice Age. *The Cryosphere*, *13*(7), 1889–1909. https://doi.org/10.5194/tc-13-1889-2019

Ogilvie, I. H. (1904). The effect of superglacial debris on the advance and retreat of some Canadian glaciers. *The Journal of Geology*, *12*(8), 722–743. https://doi.org/10.1086/621194

Østrem, G. (1959). Ice melting under a thin layer of moraine, and the existence of ice cores in moraine ridges. *Geografiska Annaler*, *41*(4), 228–230. Retrieved from https://www.jstor.org/stable/4626805

Pellicciotti, F., Stephan, C., Miles, E., Herreid, S., Immerzeel, W., & Bolch, T. (2015). Mass-balance changes of the debris-covered glaciers in the Langtang Himal, Nepal, 1974–99. *Journal of Glaciology*, *61*(226), 373–386. https://doi.org/10.3189/2015JoG13J237

Pritchard, H. D. (2019). Asia's shrinking glaciers protect large populations from drought stress. *Nature*, *569*(7758), 649–654. https://doi.org/10.1038/s41586-019-1240-1

Ragettli, S., Bolch, T., & Pellicciotti, F. (2016). Heterogeneous glacier thinning patterns over the last 40 years in Langtang Himal, Nepal. *The Cryosphere*, *10*(5), 2075–2097. Retrieved from http://www.the-cryosphere.net/10/2075/2016/. https://doi.org/10.5194/tc-10-2075-2016

R Core Team. (2019). *R: A language and environment for statistical computing*. R version 3.6.0 [Computer software manual]. Vienna, Austria. Retrieved from https://www.R-project.org/

Reid, T., & Brock, B. (2014). Assessing ice-cliff backwasting and its contribution to total ablation of debris-covered Miage glacier, Mont Blanc massif, Italy. *Journal of Glaciology*, *60*(219), 3–13. Retrieved from http://www.igsoc.org/journal/60/219/j13J045.html. https://doi.org/10.3189/2014JoG13J045

Reid, T., Carenzo, M., Pellicciotti, F., & Brock, B. (2012). Including debris cover effects in a distributed model of glacier ablation. *Journal of Geophysical Research*, *117*(D18). https://doi.org/10.1029/2012JD017795

Rounce, D. R., King, O., McCarthy, M., Shean, D. E., & Salerno, F. (2018). Quantifying debris thickness of debris-covered glaciers in the Everest region of Nepal through inversion of a subdebris melt model. *Journal of Geophysical Research: Earth Surface*, *123*(5), 1094–1115. https://doi.org/10.1029/2017jf004395

Rowan, A. V., Egholm, D. L., Quincey, D. J., & Glasser, N. F. (2015). Modeling the feedbacks between mass balance, ice flow and debris transport to predict the response to climate change of debris-covered glaciers in the Himalaya. *Earth and Planetary Science Letters*, *430*, 427–438. https://doi.org/10.1016/j.epsl.2015.09.004

Sakai, A., Nakawo, M., & Fujita, K. (1998). Melt rate of ice cliffs on the Lirung glacier, Nepal Himalayas, 1996. *Bulletin of Glacier Research*, *16*, 57–66. Retrieved from http://www.seppyo.org/bgr/pdf/16/BGR16P57.PDF

Sakai, A., Takeuchi, N., Fujita, K., & Nakawo, M. (2000). Role of supraglacial ponds in the ablation process of a debris-covered glacier in the Nepal Himalayas. *IAHS Publication*, *265*, 119–132. Retrieved from http://hydrologie.org/redbooks/a264/iahs\\text{_}264\\text{_}0119.pdf

Scherler, D., Bookhagen, B., & Strecker, M. (2011). Spatially variable response of Himalayan glaciers to climate change affected by debris cover. *Nature Geoscience*, *4*(3), 156–159. https://doi.org/10.1038/ngeo1068. Retrieved from http://www.nature.com/doifinder/10.1038/ngeo1068

Scherler, D., Wulf, H., & Gorelick, N. (2018). Global assessment of supraglacial debris-cover extents. *Geophysical Research Letters*, *45*(21), 11–798. https://doi.org/10.1029/2018GL080158

Steiner, J. F., Buri, P., Miles, E. S., & Pellicciotti, F. (2019). Supraglacial ice cliffs and ponds on debris-covered glaciers: Spatio-temporal distribution and characteristics. *Journal of Glaciology*, 1–16. https://doi.org/10.1017/jog.2019.40

Steiner, J. F., & Pellicciotti, F. (2016). Variability of air temperature over a debris-covered glacier in the Nepalese Himalaya. *Annals of Glaciology*, *57*(71), 295–307. https://doi.org/10.3189/2016AoG71A066

Thompson, S., Benn, D. I., Mertes, J., & Luckman, A. (2016). Stagnation and mass loss on a Himalayan debris-covered glacier: Processes, patterns and rates. *Journal of Glaciology*, *62*(233), 467–485. https://doi.org/10.1017/jog.2016.37

Watson, C. S., Quincey, D. J., Carrivick, J. L., & Smith, M. W. (2016). The dynamics of supraglacial ponds in the Everest region, central Himalaya. *Global and Planetary Change*, *142*, 14–27. https://doi.org/10.1016/j.gloplacha.2016.04.008

Watson, C. S., Quincey, D. J., Carrivick, J. L., & Smith, M. W. (2017). Ice cliff dynamics in the Everest region of the Central Himalaya. *Geomorphology*, *278*, 238–251. https://doi.org/10.1016/j.geomorph.2016.11.017

Watson, C. S., Quincey, D. J., Smith, M. W., Carrivick, J. L., Rowan, A. V., & James, M. R. (2017). Quantifying ice cliff evolution with multi-temporal point clouds on the debris-covered Khumbu Glacier, Nepal. *Journal of Glaciology*, 1–15. https://doi.org/10.1017/jog.2017.47

References from the Supporting Information

ASTER. (2009). NASA/METI/AIST/Japan Spacesystems And U.S./Japan ASTER Science Team *ASTER Global Digital Elevation Model*. Pasadena, CA. NASA EOSDIS Land Processes DAAC. https://doi.org/10.5067/ASTER/ASTGTM.002

Dilley, A. C., & O'Brien, D. M. (1998). Estimating downward clear sky long-wave irradiance at the surface from screen temperature and precipitable water. *Quaterly Journal of the Royal Meteorological Society*, *124*(549), 1391–1401. https://doi.org/10.1002/qj.49712454903

Heynen, M., Miles, E., Ragettli, S., Buri, P., Immerzeel, W. W., & Pellicciotti, F. (2016). Air temperature variability in a high-elevation Himalayan catchment. *Annals of Glaciology*, *57*(71), 212–222. https://doi.org/10.3189/2016AoG71A076

Hudson, D. (1966). Fitting segmented curves whose join points have to be estimated. *Journal of the American Statistical Association*, *61*(316), 1097–1129.

Juszak, I., & Pellicciotti, F. (2013). A comparison of parameterizations of incoming longwave radiation over melting glaciers: Model robustness and seasonal variability. *Journal of Geophysical Research: Atmospheres*, *118*(8), 3066–3084. https://doi.org/10.1002/jgrd.50277

Kraaijenbrink, P. D. A., Shea, J. M., Litt, M., Steiner, J. F., Treichler, D., Koch, I., & Immerzeel, W. W. (2018). Mapping surface temperatures on a debris-covered glacier with an unmanned aerial vehicle. *Frontiers in Earth Science*, *6*. https://doi.org/10.3389/feart.2018.00064

Nash, J., & Sutcliffe, J. (1970). River flow forecasting through conceptual models part I—A discussion of principles. *Journal of Hydrology*, *10*(3), 282–290. https://doi.org/10.1016/0022-1694(70)90255-6. Retrieved from http://linkinghub.elsevier.com/retrieve/pii/0022169470902556

Ragettli, S., Pellicciotti, F., Immerzeel, W. W., Miles, E. S., Petersen, L., Heynen, M., et al. (2015). Unraveling the hydrology of a Himalayan catchment through integration of high resolution in situ data and remote sensing with an advanced simulation model. *Advances in Water Resources*, *78*, 94–111. https://doi.org/10.1016/j.advwatres.2015.01.013

Shea, J., Wagnon, P., Immerzeel, W., Biron, R., Brun, F., & Pellicciotti, F. (2015). A comparative high-altitude meteorological analysis from three catchments in the nepalese himalaya. *International Journal of Water Resources Development*, *31*(2), 174–200. https://doi.org/10.1080/07900627.2015.1020417

Steiner, J. F. (2014). *Modeling ice cliff backwasting on a debris-covered glacier* (Master thesis): ETH Zurich.

Steiner, J. F., Pellicciotti, F., Buri, P., Miles, E. S., Immerzeel, W., & Reid, T. D. (2015). Modeling ice cliff backwasting on a debris covered glacier in the Nepalese Himalayas. *Journal of Glaciology*, *61*(229), 889–907. https://doi.org/10.3189/2015JoG14J194

Stigter, E. E., Wanders, N., Saloranta, T. M., Shea, J. M., Bierkens, M. F. P., & Immerzeel, W. W. (2017). Assimilation of snow cover and snow depth into a snow model to estimate snow water equivalent and snowmelt runoff in a Himalayan catchment. *The Cryosphere*, *11*(4), 1647–1664. https://doi.org/10.5194/tc-11-1647-2017

Unsworth, M., & Monteith, J. (1975). Long-wave radiation at the ground I. Angular distribution of incoming radiation. *Quarterly Journal of the Royal Meteorological Society*, *101*, 13–24.

Uppala, S. M., Kållberg, P. W., Simmons, A. J., Andrae, U., Bechtold, V. D. C., Fiorino, M., et al. (2005). The ERA-40 re-analysis. *Quarterly Journal of the Royal Meteorological Society*, *131*(612), 2961–3012. https://doi.org/10.1256/qj.04.176

Weidinger, J. T., Schramm, J. M., & Nuschej, F. (2002). Ore mineralization causing slope failure in a high-altitude mountain crest—On the collapse of an 8000 m peak in Nepal. *Journal of Asian Earth Sciences*, *21*(3), 295–306. https://doi.org/10.1016/S1367-9120(02)00080-9